Wiley
Advances in Polymer Technology
Volume 2025, Article ID 2715691, 17 pages
https://doi.org/10.1155/adv/2715691

WILEY

Research Article

Comprehensive Evaluation of NBR Sealing Performance Under Medium-Pressure Hydrogen Aging: Experimental Analysis and Predictive Model Using Convolutional Neural Network

Ahmed Nazmus Sakib,[1] **Md Monjur Hossain Bhuiyan**,[1] **Alfredo Becerril Corral**,[1] **Monsur Chowdhury**,[2] **and Zahed Siddique**[1]

[1]*School of Aerospace and Mechanical Engineering, University of Oklahoma, Norman, Oklahoma, USA*
[2]*School of Statistics, University of Georgia, Athens, Georgia, USA*

Correspondence should be addressed to Ahmed Nazmus Sakib; nazmus.sakib@ou.edu

Received 5 March 2025; Revised 22 August 2025; Accepted 1 September 2025

Academic Editor: Srijoni Sengupta

The study investigates the sealing performance of nitrile butadiene rubber (NBR) seals in hydrogen facilities, with a focus on safety and reliability through extensive experimental analysis and accelerated aging simulations. This research involved a range of characterization tests, including tensile strength, swelling, hardness, and resistivity measurements, as well as scanning electron microscopy (SEM) morphological examinations, to assess material degradation under hydrogen pressures up to 5000 psi at room temperature. The results revealed significant changes in mechanical and physical properties, including reductions in tensile strength and hardness, increased resistivity, and material swelling, all of which were attributed to hydrogen-induced structural degradation. Morphological analysis via SEM highlighted surface roughening and microcrack formation at higher pressures. A Multivariate regression model was developed to predict key properties such as tensile strength, resistivity, weight, and hardness as functions of hydrogen pressure. Additionally, a hybrid machine learning model incorporating convolutional neural networks (CNNs) for feature extraction with fully connected layers for regression was also developed, demonstrating strong predictive performance for NBR's material properties using both numerical features and SEM images. These findings contribute to the development of safer and more reliable sealing materials, crucial for the hydrogen energy industry, ensuring that seals can withstand the unique challenges posed by hydrogen storage and transportation.

1. Introduction

Hydrogen, increasingly recognized as a crucial component in the transition to clean energy, introduces distinct challenges, particularly concerning its tendency to permeate through sealing materials [1, 2]. A major concern is hydrogen's tendency to permeate through seals, potentially resulting in significant leakage risks. These risks are of paramount concern within the hydrogen industry, where even minor leaks can result in severe safety hazards, including the potential for explosive conditions [3]. This challenge stems largely from hydrogen's exceptionally small molecular size, which enables it to diffuse more readily through sealing materials compared to larger gas molecules. Unlike traditional hydrocarbons, hydrogen's compact structure makes it particularly difficult to contain, posing greater challenges for material integrity and system safety [3]. As a result, the development of advanced sealing materials and technologies becomes essential to ensure the safe and efficient use of hydrogen as a sustainable source of energy [3, 4]. These advancements need to meet the challenging requirements of hydrogen storage, transportation, and application, prioritizing both safety and efficiency [5]. This involves developing seals that can withstand extreme temperatures and resist hydrogen permeation, sustain their structural integrity under extreme pressures and temperatures, and remain durable over time. Addressing these challenges is essential for the hydrogen industry to unlock the full potential of hydrogen as a decarbonized energy system, while minimizing the associated risks [4, 6, 7].

The implications of hydrogen leakage are diverse, involving not only safety risks but also the accelerated deterioration of materials and potential environmental harm. One of the primary challenges is the degradation of materials caused by hydrogen, which can weaken the reliability of storage and transportation systems, leading to increased vulnerability to failures and additional safety hazards. A critical challenge is hydrogen embrittlement, where exposure to hydrogen gas reduces material ductility and increases susceptibility to fracture. This phenomenon is particularly problematic in sectors where structural integrity is crucial, such as aerospace and energy [8]. The combination of hydrogen-induced material degradation and embrittlement compromises the reliability of systems, increasing the risk of failures and heightening safety concerns. Research indicates that certain metals, including steel, can experience hydrogen embrittlement, emphasizing the need for thorough assessments of sealing materials [5]. Hence, to ensure hydrogen can be safely and efficiently used as a sustainable energy source, it is crucial to address these challenges by developing durable sealing materials and advanced technologies. This shows the importance of ongoing innovation in the field.

In addition to hydrogen-induced embrittlement, the purity of hydrogen gas plays a crucial role in influencing the long-term performance and degradation behavior of sealing materials. While hydrogen itself can permeate and interact with elastomeric compounds like nitrile butadiene rubber (NBR), the presence of impurities, such as water vapor, oxygen, carbon monoxide, or trace hydrocarbons, can significantly intensify chemical degradation processes. These contaminants may react with functional groups in the polymer matrix or catalyze oxidative or hydrolytic reactions at elevated temperatures and pressures, ultimately compromising the mechanical integrity and sealing effectiveness of the material [9, 10]. Understanding the effect of hydrogen purity is vital for simulating realistic service conditions, particularly in industrial hydrogen applications where gas purity may vary depending on the production or supply method. Studies have shown that even low concentrations of impurities can accelerate aging, surface cracking, and microstructural changes in elastomers over time, thereby reducing their operational lifespan and reliability. In this context, evaluating NBR under different hydrogen purities helps inform material selection and improve the design of seals that are both durable and compatible with real-world hydrogen environments.

Hydrogen's high flammability poses a serious risk, as leaks in substantial quantities, if ignited, can cause fires or explosions. Addressing these hazards necessitates a thorough understanding of how different sealing materials perform under varying hydrogen concentrations and operating conditions [11]. Sealing materials, ranging from elastomers to metals, face rigorous conditions in hydrogen environments. For example, hydrogen can permeate through materials, leading to issues like blistering in elastomeric materials, a phenomenon observed in rubbery O-rings due to rapid decompression of highly pressurized hydrogen gas [12, 13]. This emphasizes the necessity for developing specialized seals capable of withstanding the unique challenges posed by hydrogen. Given the tendency of hydrogen to permeate and degrade conventional materials, it is essential to design seals that maintain their integrity under such demanding conditions. The performance of seals is crucial in preventing hydrogen leakage and ensuring the integrity of equipment, pipelines, and hydrogen storage systems [14]. Effective seals are essential to maintain the integrity of these systems by ensuring a secure barrier that withstands high-pressure hydrogen environments [14, 15].

As the hydrogen industry aims to replace traditional energy sources, it is crucial to understand how sealing materials perform in hydrogen environments to ensure the safety, reliability, and longevity of hydrogen infrastructure [16, 17]. Proper sealing is essential to maintaining the integrity of storage, transportation, and distribution systems, preventing leaks, and mitigating potential risks associated with hydrogen's flammability and permeability [18, 19]. Research in this area seeks to reveal how hydrogen affects these seals, including how it might damage or weaken them. This knowledge is key to developing better seals that can handle the unique challenges of hydrogen. By gaining insights into these interactions, we can create materials that are more durable, ensuring the safe and effective use of hydrogen technology across different applications. NBR is a key sealing material in the hydrogen industry due to their unique properties under challenging environmental conditions [20]. It is preferred for its strong resistance to oils and chemicals, providing reliable performance in hydrogen fuel cells and storage systems where hydrocarbon oils and fuels are involved. As hydrogen technologies advance, it is crucial to study these materials extensively.

Ongoing research aims to ensure that materials can sustain their integrity and performance under the challenging conditions of high-pressure, elevated temperatures, and chemical reactivity that are common in hydrogen energy systems. This study specifically investigates (NBR), analyzing how its sealing performance is impacted by exposure to hydrogen under various operating conditions. A series of characterization tests, including tensile strength, swelling, hardness, resistivity measurements, and scanning electron microscopy (SEM) morphological analysis, were conducted to evaluate material degradation.

As sealing performance is highly nonlinear and influenced by complex interactions between pressure, temperature, and hydrogen diffusion, machine learning methods, particularly hybrid deep learning models, have been increasingly used to model these behaviors. Studies have demonstrated that convolutional neural networks (CNNs) combined with fully connected neural networks (FCNNs) are effective in capturing spatial patterns and predicting material degradation metrics with high accuracy. Inspired by these advancements, the current work applies a similar CNN-based hybrid model tailored to NBR performance in hydrogen environments [21, 22].

Building upon these advancements, the present study implements a tailored CNN–FCNN hybrid model to predict key performance properties of NBR under hydrogen exposure. The model is trained using experimental data obtained from a series of characterization tests, including tensile strength, swelling, hardness, and electrical resistivity, along with morphological analysis through SEM. This hybrid learning approach not

Table 1: Composition of NBR (40) polymer.

Filler-reinforcing	Processing aid	Antioxidant	Curing agent
Carbon Black (50)	1,2-Benzenedicarboxylic acid (6)	2-Benzimidazolethiol (2)	Sulfur (2)

Note: Numbers in () are weight ratios in %.

only enhances predictive accuracy but also provides deeper insights into how NBR degrades under hydrogen-rich conditions. Such predictive capabilities are critical for the design and selection of robust sealing materials capable of maintaining structural integrity and barrier properties under the demanding conditions of hydrogen storage and transport systems.

2. Materials and Methods

2.1. Materials. NBR is a copolymer composed of acrylonitrile and butadiene [23]. NBR is utilized in manufacturing O-rings, gaskets, and hoses that are essential in hydrogen fuel cells and hydrogen refueling stations, where robust and durable seals are crucial for operational efficiency and safety [24]. The chemical structure of NBR arises from its monomer units: acrylonitrile ($CH_2{=}CH{-}CN$) and butadiene ($CH_2{=}CH{-}CH{=}CH_2$). Through copolymerization, these monomers form a repeating unit structure along the polymer chain. The general structure of NBR can be depicted as follows:

$$-(CH_2{-}CH(CN))_x{-}(CH_2{-}CH{=}CH{-}CH_2)_y-$$

Here, x represents the proportion of acrylonitrile units, and *y* represents the proportion of butadiene units in the copolymer chain. The ratio of these units can vary, typically with acrylonitrile content ranging from 18% to 50% by weight, affecting the physical and chemical properties of the resulting NBR polymer. This structural configuration significantly influences the material's performance, particularly under medium-pressure hydrogen aging conditions, which are investigated in this study.

NBR is extensively employed in the hydrogen industry, primarily due to its remarkable resistance to gases and oils. This unique combination of properties makes NBR an ideal material for critical sealing applications in hydrogen storage and transportation systems [25]. Its exceptional mechanical strength, coupled with excellent chemical resistance, ensures the reliable containment of hydrogen by effectively preventing leaks and maintaining system pressure. These capabilities are particularly crucial in environments where temperatures and pressures fluctuate, as NBR demonstrates superior performance in maintaining the integrity and safety of hydrogen containment systems. Table 1 provides a detailed overview of the composition of NBR, highlighting the material's chemical structure and its role in delivering these desirable properties.

Carbon black was included as a reinforcing filler to enhance the mechanical properties of the NBR compound. It improves tensile strength, elasticity, and wear resistance, which are essential for maintaining seal integrity in demanding hydrogen environments. Additionally, carbon black helps reduce gas permeability, contributing to the compound's effectiveness in preventing hydrogen leakage under pressure [26, 27].

A commercial NBR O-ring was considered to carry out the experiment. But elastomeric materials of the same chemistry from different vendors can vary in residual thermal stress depending on the mode of manufacture. Therefore, NBR was subjected to an annealing process to relieve stress before exposure to high-pressure hydrogen exposure. The annealing process involves heating the NBR to a temperature of around 100°C to 120°C.

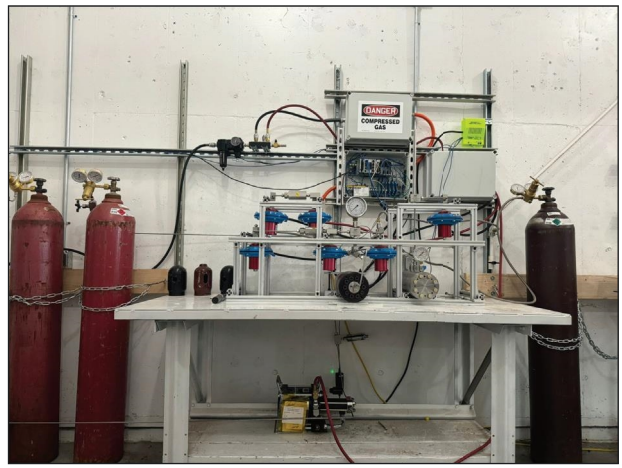

Figure 1: Experimental setup with aging chamber and accessories.

2.2. Experimental Approach. Figures 1 and 2 display the actual aging chamber and the schematic diagram of the experimental setup, respectively, used during the hydrogen charging process for the specimens. Selected samples were exposed to hydrogen gas using a commercial hydrogen gas cylinder. The pilot plant was designed keeping the provision of using nitrogen gas for flushing the chamber and tubing in between two batches. A pressure accumulator has been installed to boost the pressure. The use of pneumatic valves in conjunction with solenoid valves allows for indirect control of the hydrogen gas to ensure that no one is in the vicinity of the equipment during the charging of the samples. One of the key design criteria is to minimize gas losses during the prolonged charging of high-pressure hydrogen for aging purposes [17]. AISI 316 stainless steel alloy was used as construction material for the piping used to transport hydrogen gas, commercially available tubing, fittings, and pneumatically actuated piston valves [28]. The booster employed in the experiment was designed for high-pressure applications and allowed the use of O-ring seals made from suitable materials to contain hydrogen. While the use of polymer seals in the pressure accumulator can lead to gradual gas leakage due to material degradation, routine inspections and maintenance were performed to maintain the reliability of the experimental results. Stable operating conditions throughout the experimental period were ensured by employing a pressure transducer along with remotely operated

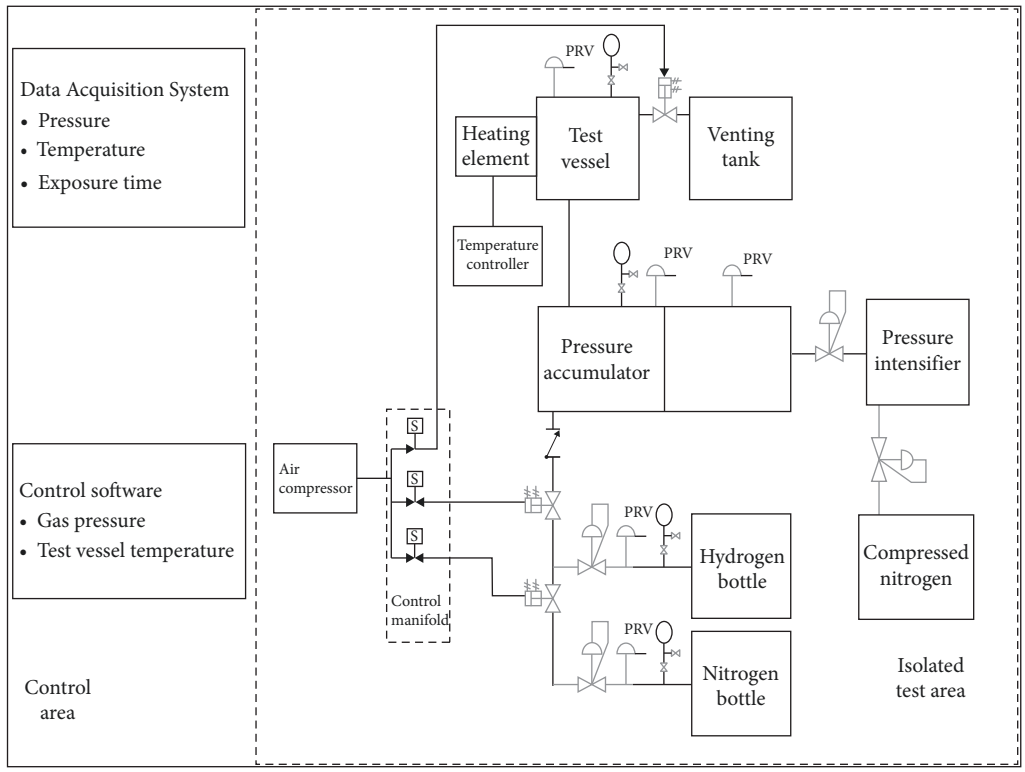

FIGURE 2: Schematic of the hydrogen assisted aging facility.

pressure regulators. The control software was configured to continuously monitor the internal pressure of the chamber and automatically adjust the inlet valve, thereby maintaining a constant hydrogen pressure during the aging tests. This software, developed in the LabVIEW environment from National Instruments, provided a flexible platform for integrating essential sensors to track parameters such as pressure, exposure time, and temperature. Once the NBR samples were prepared, they were secured in stainless steel holders, which were then placed inside a cylindrical pressure vessel for the experiment [29].

Before loading the samples, the entire system was cleaned with isopropyl alcohol (IPA). The test chamber was connected to a high-pressure setup supplied by ultrapure hydrogen and nitrogen cylinders. To eliminate residual oxygen and avoid any risk of hydrogen–oxygen explosion, the chamber was purged three times with nitrogen, with each purge followed by a complete vent at room temperature. This was followed by hydrogen purging, where the chamber was filled and vented three times at 3000 psi. After completing the purge cycles, the chamber was finally pressurized with 99.9999% ultrapure hydrogen to the designated test pressure at room temperature. The samples were then aged for 192 h under pressures ranging from 500 to 5000 psi at room temperature. Following the exposure, the deformed polymer seals were retrieved and evaluated. Three specimens of NBR were analyzed, and the mean values were reported. Mechanical and physical properties were measured both before and immediately after hydrogen exposure to determine the influence of aging on sealing performance [30, 31].

2.3. Characterization Tests to Assess Material Compatibility. A complete characterization of NBR as a sealing material in hydrogen environments; including tensile strength, swelling, hardness, resistivity, and morphology was performed to obtain insight into their behavior and durability. Tensile strength tests measure mechanical integrity and ductility, while swelling tests indicate dimensional stability and the extent of hydrogen absorption. Hardness tests show changes in rigidity and elasticity, which are critical for maintaining sealing function. Resistivity measurements determine electrical insulation capacity, which is important in specific applications. Morphology analysis using SEM identifies microstructural changes and surface damage, helping to predict long-term performance. Taken together, these tests create a baseline for assessing the reliability and suitability of NBR as sealing materials in hydrogen service [29].

2.3.1. Tensile Strength Test. The tensile strength of NBR specimens was examined to determine the effect of hydrogen permeation, following ASTM D412, the standard method for tensile testing of plastics. NBR samples were subjected to uniaxial tension until failure, providing data on both strength and ductility. The tests were carried out at room temperature with a crosshead speed of 0.083 mm/s to ensure consistency and to avoid thermal effects on the results. The main parameter measured was the ultimate tensile strength (UTS), representing the maximum stress the material can withstand before necking. This information revealed how hydrogen exposure influences the plastic deformation capability of the material. A reduction in ductility indicates a tendency toward brittleness, which increases the risk of failure under applied stress [32].

2.3.2. Hardness Test. The hardness test is an important step in assessing the mechanical performance of O-ring seals, especially after exposure to hydrogen. It is performed according to ASTM D2240, Standard Test Method for Rubber Property —Durometer Hardness, which outlines the procedure for measuring the hardness of elastomeric materials commonly used in seals. In this method, a durometer is applied perpendicularly to the specimen surface, and the resistance to indentation is recorded as the hardness value. This value reflects the material's elasticity and its ability to recover its shape after deformation. For NBR aged in hydrogen, the test is particularly relevant as it identifies changes in rigidity that may affect sealing capability. A reduction in hardness indicates softening of the material, which can compromise sealing effectiveness. Results from this test, following ASTM D2240, provide critical information on whether the aged O-rings retain sufficient mechanical integrity to function as reliable seals or if hydrogen exposure has led to performance degradation [31].

2.3.3. Resistivity Analysis. Resistivity testing is a key method for evaluating the performance of polymer-based seals, such as O-rings, after hydrogen exposure. Conducted in line with ASTM D257, Standard Test Methods for DC Resistance or Conductance of Insulating Materials, the test assesses changes in the electrical insulation properties of polymers, which typically possess very high resistivity. This property is important in applications where electrical insulation and material stability are critical. For hydrogen-aged seals, specimens are prepared with dimensions of 70 mm in diameter and 2 mm in thickness as specified in the standard. The samples are placed between four electrodes to ensure proper contact, after which a constant voltage of 100 VDC is applied for 60 s to stabilize the current and minimize transient effects. Resistance is measured using a high-sensitivity ohmmeter, and volumetric resistivity is then calculated. A significant reduction in resistivity may indicate deterioration in material structure or integrity, while values comparable to unaged samples suggest that the polymer has retained its insulating performance. As a nondestructive technique, resistivity analysis provides valuable information on durability and functional reliability, linking electrical property variations to the effects of hydrogen exposure and helping determine the long-term suitability of NBR seals in demanding service environments [33, 34].

2.3.4. Morphology Analysis. Morphology analysis using (SEM) is a critical aspect of characterizing the performance of NBR seals subjected to hydrogen aging. This analysis provides insights into the structural and surface changes that occur in polymer materials under specific environmental conditions. The primary objective of this analysis is to understand how hydrogen exposure affects the microstructural properties of these seals, which is important for assessing their suitability and durability in practical applications. When polymer seals are exposed to hydrogen, various physical and chemical changes can take place at the micro and nanoscale levels. These changes can significantly impact the material's performance, including its mechanical strength, flexibility, and sealing efficiency. The hydrogen-aged polymer seals were carefully sectioned, coated, and prepared for electron microscopy. Once prepared, SEM imaging was conducted. This involves setting up the microscope with optimal parameters such as acceleration voltage and focus to capture high-resolution images. The focused beam of electrons in SEM interacts with the sample, producing secondary electrons that render a detailed view of the surface morphology. These images provide information on surface roughness, which can influence how the seal interacts with other materials and its overall sealing performance. The images also reveal the presence of microcracks, voids, or other forms of degradation that could influence the seal's integrity. Such defects are critical to identify, as they can lead to seal failure under operational conditions.

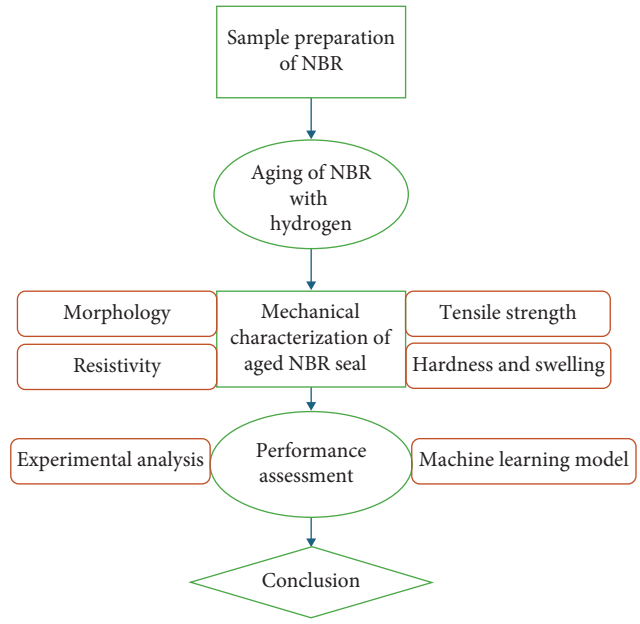

FIGURE 3: Block diagram of the workflow process.

Another key aspect that SEM analysis sheds light on is the changes in porosity and crystallinity of the polymer. These factors greatly affect the mechanical properties of the material. An increase in porosity weakens the material strength, while changes in crystallinity could alter its flexibility. Additionally, SEM can detect chemical alterations in the polymer structure due to hydrogen exposure. These alterations could potentially impact the material's resistance to gaseous hydrogen. The insights gained from this analysis guide material selection, design considerations, and processing techniques, ensuring that the polymer seals used in various applications are durable, efficient, and suited to the specific challenges posed by the operational environments [35, 36]. Figure 3 represents the block diagram of the investigation.

3. Results and Discussion

3.1. Characterization of Seals Under Hydrogen Environment. This section presents a detailed analysis of NBR sealing materials subjected to medium-pressure hydrogen aging, focusing on the characterization of NBR samples after exposure to the hydrogen environment. The focus is on evaluating how these seals perform and degrade in a hydrogen environment through

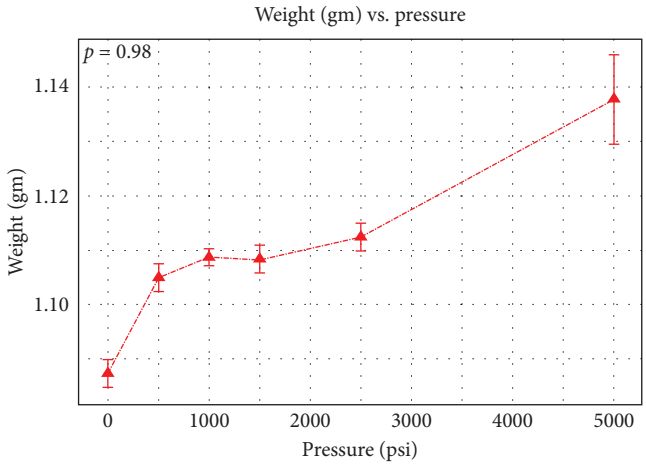

FIGURE 4: Change of weight (%) of NBR with increasing hydrogen pressure.

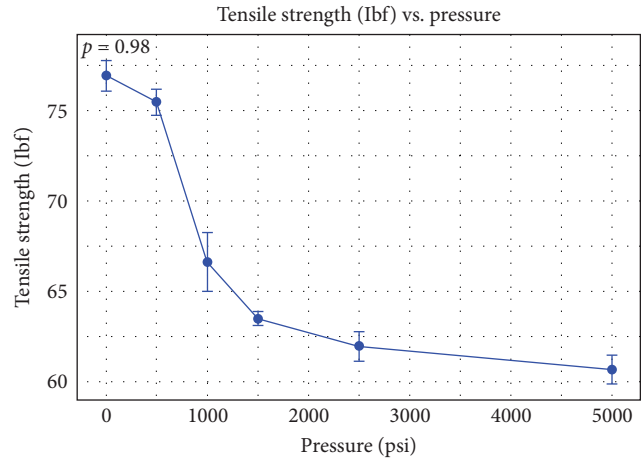

FIGURE 5: Change of tensile strength of NBR at increasing hydrogen pressure.

various characterization tests. These tests include measurements of swelling, tensile strength, resistivity, hardness, and morphological analysis of the NBR seals. The properties at 0 psi represent the original state of the virgin polymer, serving as a baseline to evaluate the effects of hydrogen aging, with the highest pressure tested being 5000 psi. Each test provides critical insights into how hydrogen exposure impacts the material's properties and integrity, which is essential for assessing its effectiveness and durability in hydrogen applications. Three sets of tests at each respective pressure were carried out to assess if any property is statistically significant and requires additional tests.

3.1.1. Swelling. Figure 4 depicts the change in weight of NBR as a function of hydrogen pressure following 192 h of aging. The increase in mass and volume is attributed to hydrogen molecules infiltrating the amorphous regions of the NBR. The trend continues with further increases in pressure, reaching a peak weight at 5000 psi. This phenomenon is closely linked to the microstructure of NBR, where the amorphous regions provide pathways for hydrogen diffusion. This phenomenon of weight increase due to gas exposure and subsequent swelling in polymers was also observed in similar studies. Cross-linked hydrogels exhibit substantial swelling when exposed to gases or solvents as they absorb gas molecules. This absorption causes the polymer chains to expand, resulting in an increase in volume and weight due to gas uptake [37]. Similarly, Amberlite polymers exposed to organic solvents such as ethanol and heptane shows an increase in weight and volume as these solvents penetrate the polymer matrix. The degree of swelling and mass increase varies with the type of solvent and the polymer's porosity, which dictates how much the polymer can absorb [38]. The swelling of polymers exposed to high-pressure gases like CO_2, and methane has also been observed before [39]. From Figure 4, it is observed that at low pressures (0 to 1500 psi), the weight gain is relatively modest, which suggests that the hydrogen uptake is limited by the initial availability of free volume in the polymer matrix. However, as the pressure increases, particularly at 3000 psi, a significant rise in weight is observed. This suggests a threshold effect where the free volume in the amorphous regions of NBR becomes more saturated with hydrogen, leading to greater expansion and absorption. This process results in a volume expansion and an increase in weight, a phenomenon critical in applications like hydrogen gas seals where polymer-hydrogen interactions affect sealing integrity. Being a polar elastomer, NBR is more prone to hydrogen uptake under high-pressure conditions, with the highest weight change observed at 5000 psi due to pronounced polymer swelling.

3.1.2. Tensile Strength. As shown in Figure 5, the tensile strength of NBR varies with hydrogen pressure after 192 h of aging. Initially, the tensile strength decreases only slightly up to around 500 psi, but beyond this point, a more consistent decline is observed as the hydrogen pressure increases. This reduction in tensile strength is indicative of the detrimental effects of hydrogen on the polymer structure. At higher pressures, hydrogen diffusion into the NBR matrix can lead to polymer chain scission, cross-linking, or plasticization, which weakens the material's mechanical properties. This phenomenon, often referred to as hydrogen embrittlement, where prolonged exposure to high-pressure hydrogen environments causes degradation in elastomeric materials, resulting in a loss of tensile strength and overall durability.

A similar study found that when NBR was exposed to hydrogen pressures up to 70 MPa, its tensile strength decreased significantly. This reduction was attributed to hydrogen diffusion into the polymer matrix, which led to the formation of microvoids, ultimately compromising the material's mechanical integrity [40]. In another study, it was found that tensile strength in silicone rubber decreased when exposed to gases like CO_2 and methane due to gas diffusion and plasticization of the polymer matrix [41, 42]. Therefore, under high-pressure, hydrogen molecules diffuse into the NBR matrix. This leads to swelling, as the polymer chains are forced apart by the gas molecules. The ingress of hydrogen creates microvoids within the polymer structure. These voids act as stress concentrators, weakening the material. High pressure can break cross-links between polymer chains. This reduces the network integrity, further compromising mechanical properties. Hydrogen can

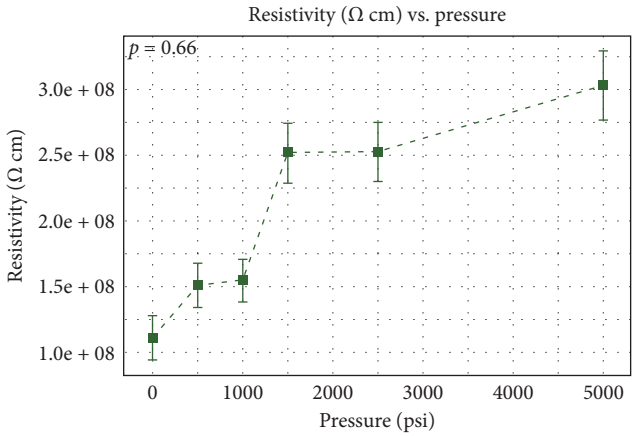

FIGURE 6: Change of resistivity of NBR at increasing hydrogen pressure.

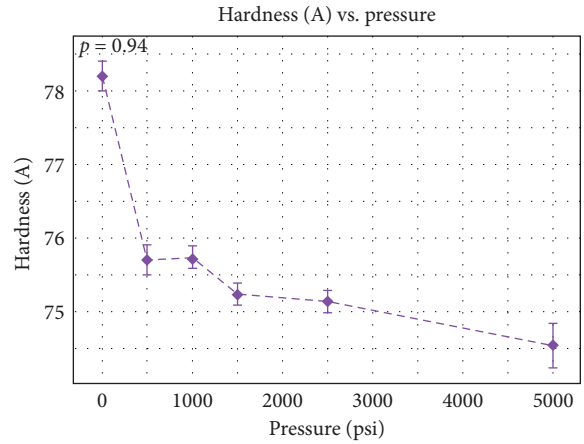

FIGURE 7: Change of hardness of NBR at increasing hydrogen pressure.

interact with the nitrile groups (—CN) in the polymer, leading to further degradation of the polymer structure. Here is a simplified diagram showing the possible paths in polymer structure where void formation can take place as follows:

$$-CH_2-CH(CN)-CH_2-CH=CH-CH_2-CH_2-CH(CN)-CH_2-CH=CH-CH_2-$$
$$\uparrow \quad \uparrow \quad \uparrow \quad \uparrow \quad \uparrow$$

Microvoids and swelling from hydrogen permeation

These structural changes may be further analyzed to explain the observed decrease in tensile strength [40].

3.1.3. Resistivity. Figure 6 demonstrates the relationship between pressure and resistivity in NBR, showing that resistivity increases as pressure rises. This behavior can be explained as hydrogen penetration into the NBR matrix, leading to microvoid formation and swelling. As hydrogen permeates the polymer, it induces physical expansion, which separates conductive filler particles and disrupts conductive pathways, resulting in an increase in resistivity. It is also observed that pressure-induced densification of polymer chains enhances the overlap between molecular orbitals, promoting charge transport and increasing resistivity. Although hydrogen exposure does not break primary chemical bonds but induces physical alterations such as increased free volume and reduced cross-link density. These structural disruptions may impact the rise in resistivity. The relatively stable behavior of NBR's resistivity under pressure can also be explained by its copolymer structure. The acrylonitrile component in NBR likely enhances chemical resistance and maintains the polymer's integrity, mitigating the hydrogen-induced degradation.

These findings are consistent with earlier studies. Fujiwara [43] observed significant volume expansion and increased resistivity in NBR due to hydrogen absorption, confirming that hydrogen can disrupt the polymer matrix through microvoid formation. Similarly, Theiler et al. [44] demonstrated that NBR's resistivity increases under high-pressure hydrogen environments, a result of polymer matrix disruption and filler particle separation. Additionally, studies on other polymers, including polyethylene and polypropylene, have also demonstrated similar increases in resistivity when exposed to gases such as hydrogen and CO_2. The gas-induced swelling in these polymers supports the general conclusion that gas permeation leads to increased resistivity due to the disruption of conductive pathways [45].

3.1.4. Hardness. Figure 7 demonstrates the decreasing trend in the hardness of NBR as a function of increasing hydrogen pressure. The hardness of the unaged NBR is initially measured at approximately 78 Shore A, but as hydrogen pressure rises to 5000 psi, the hardness gradually decreases to around 75 Shore A. This consistent decline in hardness suggests that elevated hydrogen pressures significantly affect the mechanical integrity of NBR. This behavior can be explained by the penetration of hydrogen molecules into the elastomeric matrix of NBR, resulting in microstructural changes. Hydrogen has the ability to diffuse into the amorphous regions of elastomers, leading to swelling and disruption of the polymer's cross-link network. As gas molecules permeate into the polymer, increasing the free volume and forcing the polymer chains apart. This phenomenon weakens the internal cohesion between chains, reducing the material's stiffness and, consequently, its hardness. In NBR, the nitrile groups (—CN) in the copolymer with butadiene can absorb hydrogen, exacerbating this softening effect. As pressure increases, more hydrogen diffuses into the polymer, resulting in greater chain separation, decreased cross-link density, and further reduction in hardness.

The trend observed in this plot is consistent with previous studies on the behavior of elastomers and polymers under high-pressure gas environments. A study on ethylene propylene diene monomer (EPDM) under high-pressure CO_2

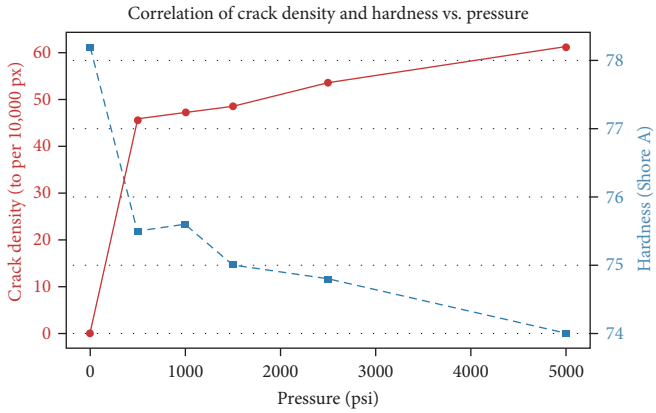

FIGURE 8: Comparison between crack density and hardness across NBR.

exposure observed a similar reduction in hardness. In this case, CO_2 penetrated the EPDM matrix, causing a swelling effect that reduced the material's stiffness and hardness due to increased chain mobility and disruption of cross-linked networks [45]. Similarly, studies on polyurethane under high-pressure nitrogen exposure have also reported a decrease in hardness, attributed to the plasticization effect of gas diffusion. Nitrogen molecules, like hydrogen, permeate the polymer structure, causing swelling and a corresponding reduction in hardness as the internal structure of the polymer becomes less rigid [39]. Moreover, the softening of NBR under high-pressure hydrogen can be attributed to hydrogen embrittlement, a phenomenon typically observed in both metals and polymers. In this context, hydrogen absorption induces microvoids and defects in the polymer matrix. These defects act as stress concentrators, further weakening the material. Cross-link scission may occur in severe cases, reducing the elastomer's ability to retain its mechanical integrity under load. As the pressure increases, hydrogen molecules can penetrate deeper into the material, exacerbating the softening effect and amplifying the reduction in hardness. Flaconnèche et al. [46] explored gas transport properties in various polymers and reported that gas-induced swelling leads to a decline in hardness, especially under high-pressure conditions where gas absorption is maximized [43, 44, 47].

Figure 8 presents a direct comparison between crack density and hardness across increasing hydrogen pressures. As pressure increases, the crack density sharply rises, while hardness consistently declines. This inverse relationship demonstrates that the morphological degradation observed in the SEM images—quantified as increasing crack density—correlates strongly with the mechanical softening of the material. The formation and propagation of cracks weaken the integrity of the NBR matrix, disrupt load-bearing continuity, and contribute to reduced surface resistance to indentation. Thus, the decreasing hardness of NBR under hydrogen exposure is not only chemically induced through molecular interactions but is also morphologically manifested through increased cracking, confirming a strong structure-property relationship under high-pressure hydrogen environments.

3.1.5. Morphology. The primary goal of this study is to evaluate the effect of increasing hydrogen pressure on the morphological integrity of NBR by analyzing the formation and propagation of cracks under different pressure conditions. By segmenting SEM images and quantitatively analyzing crack formation, we aim to gain insights into the failure mechanisms of the material when exposed to hydrogen. Understanding these changes is critical for sealing systems, where crack propagation can significantly impact material performance. To achieve the objective, we employed a combination of multilevel Otsu thresholding and watershed segmentation for crack detection. Multilevel Otsu thresholding is used to identify intensity-based regions in the images, which are then refined using watershed segmentation to improve precision in identifying crack boundaries. The morphological closing operation helps reduce noise and enhance image features by filling small gaps. These techniques allow for a robust analysis of crack formation across different pressures, providing a clear visualization of material degradation. Multilevel Otsu thresholding works by dividing the pixel intensity range into multiple classes. This allows for distinguishing between regions of interest (such as cracks) and the background more effectively compared to simple binary thresholding. The watershed algorithm is a powerful segmentation technique, particularly when dealing with overlapping objects or features, like cracks, which require fine delineation. Figure 9 shows the segmented images of NBR under different pressures using the techniques described. The combination of Otsu thresholding and watershed segmentation is ideal for this study because it balances the need for precision in crack detection with the ability to handle noise and overlapping regions effectively. Cracks in materials like NBR often appear as thin, irregularly shaped regions, making them difficult to detect using basic thresholding techniques. The watershed method excels in this scenario because it treats image intensity as a topological surface, enabling better separation of closely packed cracks or defects. Furthermore, the multilevel thresholding aspect allows for segmentation of different intensity levels, which is particularly useful in detecting cracks at varying depths and severities within the material.

The segmented images distinctly reveal the progression of crack formation with increasing pressure. At lower pressures, such as 0 psi and 500 psi, few cracks are visible, indicating that the material remains relatively intact. However, as pressure increases to 1500 psi and beyond, the number of cracks increases significantly, as evidenced by the prominent white regions in the segmented images. This suggests that higher pressures are inducing more extensive mechanical failure in the material, leading to the formation and growth of cracks.

The black areas in the images represent intact material, while the white areas correspond to detecting cracks or regions of damage. The crack quantification data in Figure 10 reveals a sharp increase in the number of cracks as pressure increases. At 0 psi, the material shows very few cracks, but at 500 psi, the cracks begin to form more frequently. By 5000 psi, the material has accumulated a significant number of cracks, indicating substantial structural degradation.

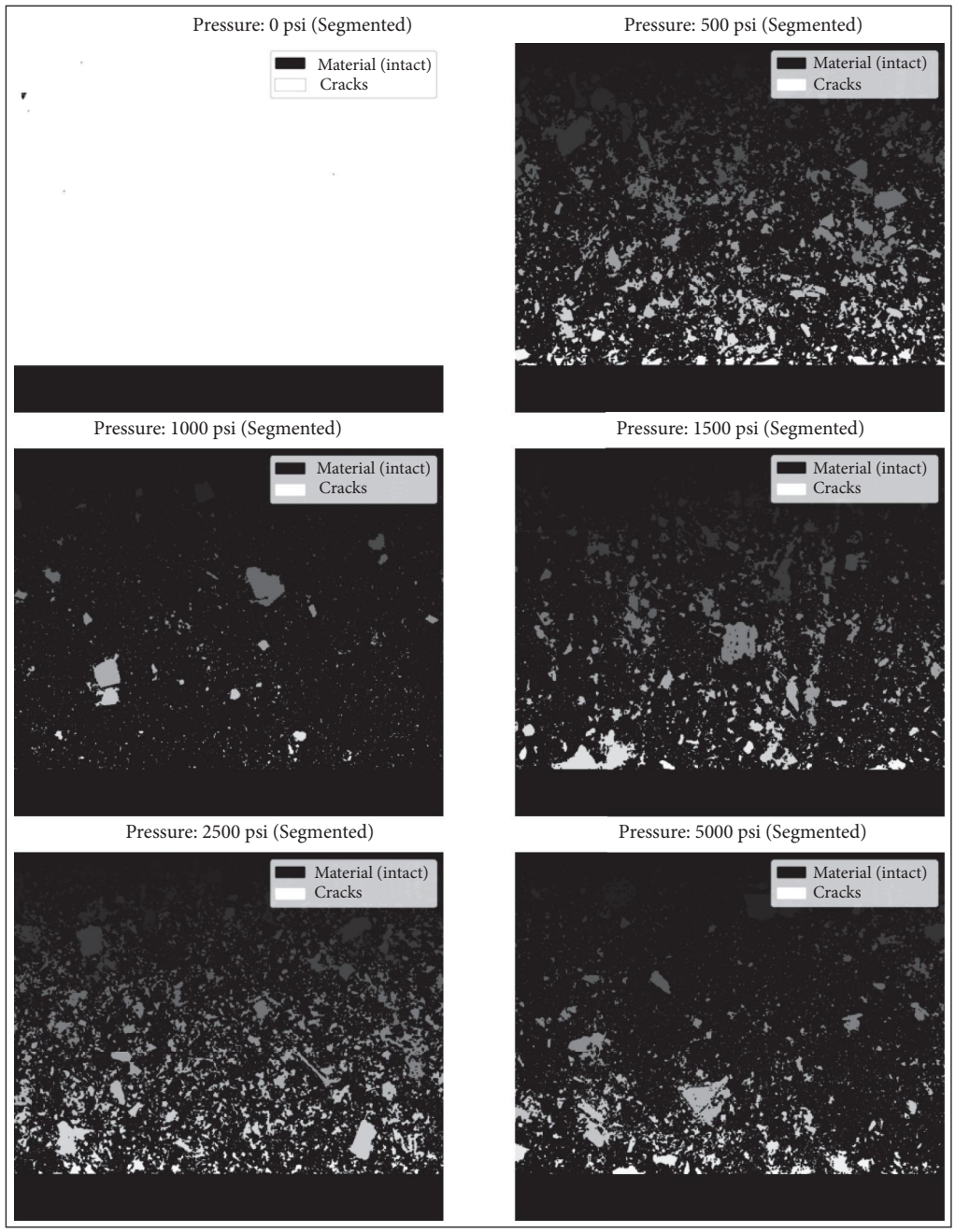

Figure 9: Segmented images of NBR under different pressures.

The study demonstrates that NBR undergoes significant morphological changes under high pressure, leading to crack formation and propagation. The segmented images and crack quantification provide crucial insights into how NBR behaves under increasing hydrogen pressure. At low pressures, NBR demonstrates good resistance, with minimal cracking. However, at higher pressures, the material becomes significantly more brittle, leading to extensive crack formation. This behavior is consistent with findings from similar studies, where elastomeric materials exposed to hydrogen at high pressures exhibit embrittlement and failure due to crack propagation.

To further strengthen the quantitative morphological assessment, crack density was calculated as the number of cracks per 10,000 pixels for each pressure condition in Figure 11. The results indicate a consistent increase in crack density with rising hydrogen pressure, supporting the trend observed in the segmentation results. At 0 psi, the material exhibits no significant cracks. However, crack density rises sharply at 500 psi and continues to increase with pressure, reaching over 60 cracks per 10,000 pixels at 5000 psi. This quantification confirms that hydrogen exposure significantly compromises the surface integrity of NBR, leading to progressive microcrack formation.

3.2. Hydrogen Absorption Into the NBR O-Ring Matrix. The hydrogen absorption into the NBR O-ring matrix was

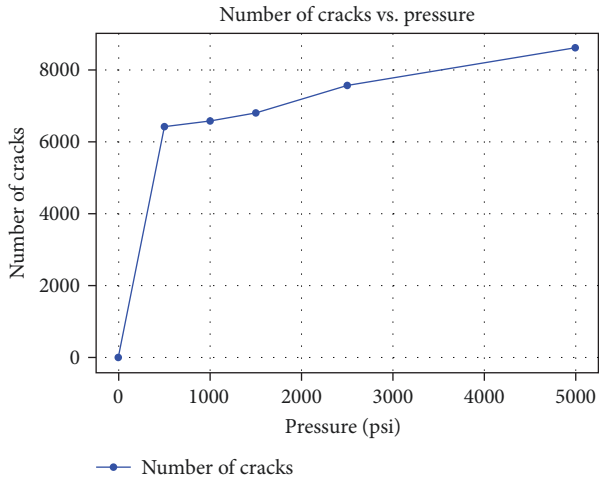

FIGURE 10: Crack quantification data of NBR material at different hydrogen pressure.

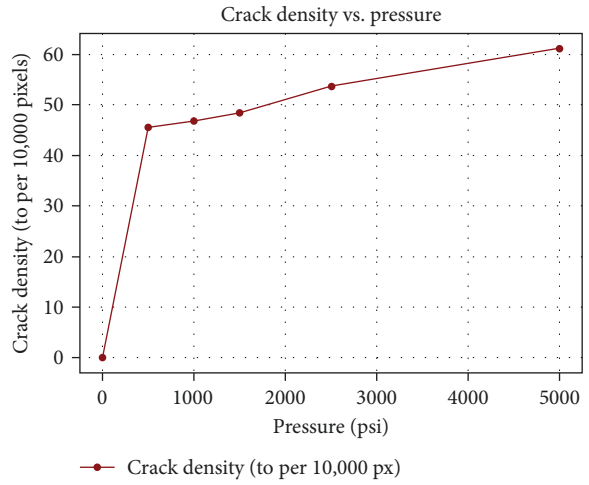

FIGURE 11: Density of crack across NBR material at different hydrogen pressure.

quantitatively evaluated under different applied hydrogen pressures using a higher-order nonlinear model, combining the effects of surface adsorption and bulk diffusion. The focus is on calculating the mass of hydrogen absorbed based on the diffusion depth, solubility, and the geometry of the O-ring.

The solubility of hydrogen in NBR is modeled using an extended form of Henry's Law, which introduces nonlinear terms to account for saturation effects at higher pressures. This is considered because, at high-pressure, hydrogen absorption in polymers like NBR begins to deviate from linear behavior as the material reaches a saturation point. The equation used for solubility is as follows:

$$C = \frac{K_H \cdot P}{1 + \alpha \cdot P + \gamma \cdot P^3},$$

where

- C is the solubility of hydrogen in NBR (mol/m^3), which represents how much hydrogen the NBR material can hold at a given pressure.
- K_H = Henry's Law constant (31.4 mol/m^3) for hydrogen solubility in NBR [48].
- P is the aging pressure (MPa) applied to seals by hydrogen.
- $\alpha = 0.01\ \text{MPa}^{-1}$; introduces first-order nonlinear effects in solubility to model deviations from the ideal gas law at high pressures [49, 50].
- $\gamma = 10^{-6}\ \text{MPa}^{-3}$ accounts for higher-order nonlinear effects, particularly saturation behavior, which occurs as the material approaches its absorption capacity [49, 50].

The diffusion of hydrogen into the NBR polymer is modeled as a pressure-dependent process, as diffusion rates vary with the applied pressure. Both linear and quadratic pressure terms were introduced to include the influence of pressure on the diffusion coefficient. The equation is as follows:

$$D(P) = D_0 \cdot (1 + \beta \cdot P + \gamma 2 \cdot P^2),$$

where

- $D_0 = 10^{-10}\ \text{m}^2/\text{s}$ is the baseline diffusion coefficient for hydrogen in NBR at standard conditions [48].
- $\beta = 0.001\ \text{MPa}^{-1}$ is the pressure dependence factor, capturing the linear increase in diffusion rate as pressure rises [49, 50].
- $\gamma_2 = 0.0001\ \text{MPa}^{-2}$ is a higher-order pressure-dependent term to account further changes in diffusion rates at high pressures [50].

The diffusion depth (δ) is calculated using Fick's Law to determine how deeply hydrogen penetrates the NBR material. This relates the diffusion coefficient and time to the depth of penetration. The diffusion depth directly affects the volume of the material that absorbs hydrogen, and thus impacts the total mass of hydrogen absorbed.

$$\delta = \sqrt{\{2 \cdot D(P) \cdot t\}},$$

where

- δ is the diffusion depth (meters) representing how far hydrogen diffuses into the NBR.
- $D(P)$ is the pressure-dependent diffusion coefficient.
- t = 192 h (691,200 s) is the aging time over which the hydrogen exposes

Subsequently, the volume of the diffusion region (V_d) was calculated based on the geometry of the O-ring using the following formula. This equation calculates the volume of the region into which hydrogen diffuses. It accounts for the cross-sectional area of the O-ring and the diffusion depth, which are to determine the total volume of the material that is exposed to hydrogen.

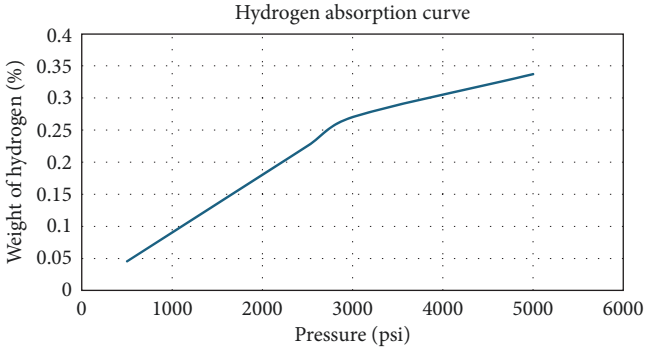

FIGURE 12: Absorption pattern of hydrogen with pressure.

$$V_{\mathrm{d}} = \pi \cdot \frac{\left\{ d^2_{\{\mathrm{out}\}} - d^2_{\{\mathrm{in}\}} \right\}}{4} .\delta$$

where

- $d_{\mathrm{out}} = 0.03$ m is the outer diameter of the O-ring.
- $d_{\mathrm{in}} = 0.025$ m is the inner diameter of the O-ring.
- δ is the calculated diffusion depth with different pressure.

With the solubility (C) and the volume of the diffusion region (V_{d}) calculated, the moles of hydrogen absorbed (nH) can be determined using the following formula:

$$\mathrm{nH} = C \times \mathrm{V_d},$$

where

- nH is the number of moles of hydrogen absorbed into the NBR material.
- C is the solubility of hydrogen at a given pressure, calculated in Step 1.
- V_{d} is the volume of the diffusion region.

Finally, the mass of hydrogen absorbed (M_{H}) is calculated by converting the number of moles of hydrogen absorbed into mass. The molecular weight of hydrogen (2.016 mg/mol} is used for this conversion.

$$M_{\mathrm{H}} = \mathrm{nH} \times 2.016\ \mathrm{mg/mol},$$

where

- M_{H} is the mass of hydrogen absorbed, measured in milligrams.
- nH is the number of moles of hydrogen absorbed.
- 2.016 is the molecular weight of hydrogen.

Figure 12 shows the theoretical relationship between pressure (MPa) and the change of weight (%) in NBR O-rings, using the higher-order nonlinear model. The trend exhibits a nonlinear increase in hydrogen absorption as pressure increases, particularly noticeable at higher pressures. This behavior is consistent with the expected saturation of hydrogen in the NBR material, where the absorption capacity of the polymer slows down as the pressure approaches higher values.

The nonlinear absorption behavior observed, where hydrogen absorption slows down at higher pressures, is consistent with findings from previous studies on gas permeability and solubility in polymers. Flaconnèche et al. [46] demonstrated on polyethylene, polyamide 11, and poly(vinylidene fluoride) that gas absorption tends to show a linear increase at lower pressures but levels off at higher pressures due to saturation effects in the polymer matrix [46].

4. Machine Learning Model to Predict Tensile Strength

4.1. Data Variables and Model. The dataset consists of observations for four response variables—tensile strength, resistivity, weight, and hardness—and one predictor, pressure. The dependent variables are continuous, and a multivariate linear regression (LR) model was applied to explore the influence of pressure on each material property. Multivariate regression is a powerful statistical technique used to model relationships between multiple dependent variables and one or more independent variables. A multivariate regression model is used when we have more than one dependent variable (also called response variables) that we are trying to predict or explain using one or more independent variables (predictors). The general form of a multivariate regression model is as follows:

$$Y = X\beta + \varepsilon,$$

where

- Y is an $n \times p$ matrix of dependent variables (with n observations and p response variables).
- X is an $n \times k$ matrix of independent variables (with k predictor variables, including a column of ones if we have an intercept).
- β is a $k \times p$ matrix of regression coefficients (one set of coefficients for each response variable).
- ε is an $n \times p$ matrix of error terms (representing the residuals or noise in the data).

The fitted equation for each response variable Y_j (where $j = 1, 2, \ldots, p$) can be written as follows:

$$Y_j = \beta_{0j} + \beta_{1\mathrm{j}} X_1 + \beta_{2j} X_2 + \ldots + \beta_{\mathrm{kj}} X_{\mathrm{k}} + \varepsilon_{\mathrm{j}}$$

Here, β_{0j} is the intercept for the j-th response variable, and $\beta_{1\mathrm{j}}$ are the coefficients for the
i-th predictor in relation to the j-th response variable.

4.2. Model Output Analysis

4.2.1. Scatter Plot With Regression Lines. The scatter plot at Figure 13 visualizes the relationship between Pressure (independent variable) and four material properties: tensile strength, resistivity, weight, and hardness (dependent variables). The regression lines fit to the data points represent the linear

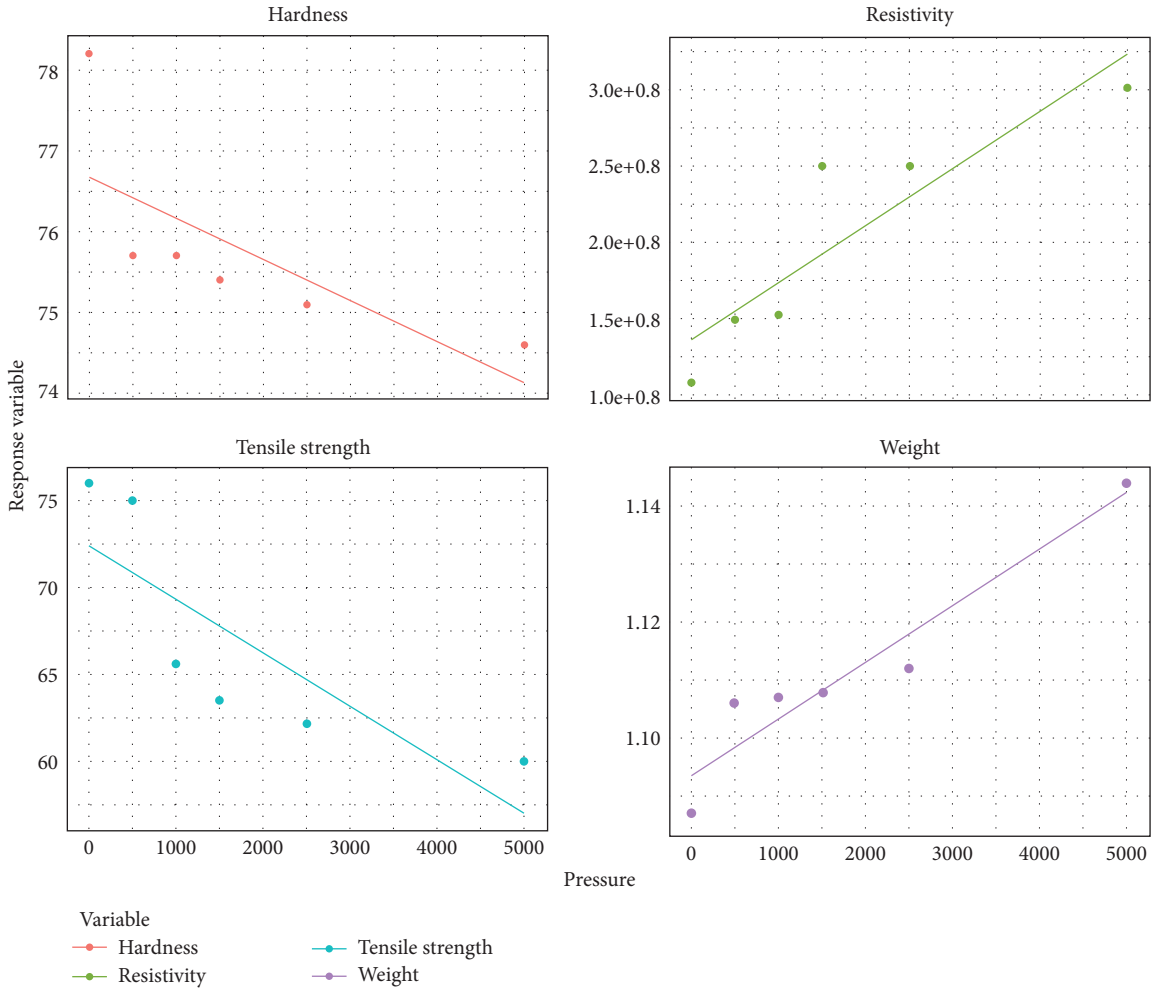

FIGURE 13: Scatter plot of material properties with pressure.

relationship between pressure and each property. The relationships between various material properties and pressure reveal distinct linear trends.

The relationships between various material properties and pressure reveal distinct linear trends. For tensile strength vs. pressure, a negative linear trend indicates that higher pressure values correspond to lower tensile strength, suggesting that increasing pressure weakens the material's ability to resist tensile stress, making it more prone to failure or deformation. In contrast, resistivity vs. pressure exhibits a positive linear trend, indicating that as pressure increases, the material's resistivity also rises, suggesting decreased electrical conductivity, which could affect performance in applications requiring conductivity. Additionally, the weight vs. pressure relationship shows a positive linear trend, indicating that as pressure increases, the material's weight also rises, likely due to increased density or mass from compression or structural changes, potentially impacting usability where weight is critical. Last, the hardness vs. pressure relationship reveals a negative linear trend, suggesting that higher pressure leads to decreased hardness, implying that the material may become softer or more prone to deformation, thus reducing its durability in high-pressure applications.

The results of the regression analysis are presented in four separate model summaries, one for each response variable. These summaries include the estimated coefficients, p-values, and R^2 values to assess the model fit.

4.3. Model Strength Analysis. The analysis results from Table 2 show that pressure has a statistically significant impact on multiple material properties, with varying effect sizes and model fits. For tensile strength, the pressure coefficient is −0.0031, indicating a significant negative effect. This implies that tensile strength decreases modestly by approximately 0.0031 units for every unit increase in pressure, with the model explaining 66.56% of the variance ($R^2 = 0.6656$). In the case of resistivity, the pressure coefficient of 37,306 reveals a substantial positive relationship between pressure and resistivity, where resistivity increases significantly as pressure rises. This model demonstrates a strong fit, accounting for 80.61% of the variance ($R^2 = 0.8061$). The relationship between weight and pressure is also positive and highly significant, though the effect size is relatively small. Each unit increase in pressure leads to an increase in weight by 9.77e–06 units, and this model shows the strongest predictive power, explaining 91.14% of the variance ($R^2 = 0.9114$). For hardness, however, the results indicate

Table 2: Regression results for pressure impact on various properties.

Property	Coefficient	Estimate	p-Value	R^2
Tensile strength	Pressure	−0.0031	0.0477	0.6656
Resistivity	Pressure	37,306	0.0151	0.8061
Weight	Pressure	9.77e−06	0.0030	0.9114
Hardness	Pressure	−0.00051	0.0971	0.5379

Table 3: CNN model performance for predicting material properties under hydrogen exposure.

Material property	Original CNN MSE	Residual CNN MSE
Tensile strength	7.571e+01	4.561e+01
Hardness	4.450e+00	2.960e+00
Resistivity	1.225e+15	5.161e+15
Swelling	2.200e−04	2.640e−04

a nonsignificant negative relationship with pressure. The pressure coefficient of −0.00051, combined with a p-value of 0.0971, suggests that while hardness decreases slightly with increasing pressure, the relationship lacks statistical significance, and the model explains only 53.79% of the variance ($R^2 = 0.5379$). This implies that other factors beyond pressure may be more influential in determining hardness. Overall, pressure plays an important role in determining resistivity and weight, as reflected in the high R^2 values, while its effect on tensile strength is significant but smaller. This study demonstrates that pressure is a significant factor influencing the material properties of tensile strength, resistivity, weight, and hardness. The regression models revealed varying degrees of sensitivity to pressure, with resistivity and weight showing strong relationships. These findings provide valuable insights for industries where pressure variations are common, guiding material selection and engineering design based on specific performance criteria under pressure conditions.

Future research could explore nonlinear effects of pressure or consider other environmental variables to further elucidate the relationships between material properties and external conditions.

4.4. CNN. We developed a CNN model to predict four critical material properties—tensile strength, resistivity, swelling (weight), and hardness—based on grayscale SEM images of NBR materials exposed to hydrogen environments. The objective was to utilize deep learning for feature extraction directly from high-resolution morphology, eliminating the need for manual descriptors and enabling end-to-end prediction.

4.5. Model Architecture and Hyperparameter Tuning. The initial architecture consisted of three convolutional layers followed by batch normalization, max pooling, and fully connected dense layers. A systematic hyperparameter optimization strategy was employed to identify the ideal number of filters (ranging from 32 to 128), convolutional depth (2–4 layers), and learning rate (0.0001–0.01). The final model was trained over 10 epochs using the Adam optimizer, with performance evaluated on an independent test set using Mean Squared Error (MSE).

To address concerns about model capacity, we revised the architecture to include five convolutional layers with residual connections, enabling deeper feature extraction and mitigating vanishing gradient issues. This improved architecture led to notable gains in prediction accuracy across most material properties. As shown in Table 3, the residual CNN reduced the MSE for tensile strength from 75.71 to 45.61, for hardness from 4.45 to 2.96, and slightly improved swelling prediction. Although resistivity prediction remains a challenge due to its extreme numeric scale, performance improved relative to the baseline.

4.6. Benchmarking Against Traditional Models. To support our claim that the CNN model outperforms traditional methods, we conducted a comparative analysis using LR and Support Vector Regression (SVR) as baselines. Table 4 presents MSE values across the same train-test split. The CNN model consistently achieved lower error than both LR and SVR for hardness and swelling and showed improved performance for tensile strength and resistivity as well. These results confirm the value of image-based feature learning and support the use of CNNs for predictive modeling in materials science.

4.7. Integration With CNN-Hybrid Modeling Approaches. Our approach builds on recent advances in CNN-hybrid modeling, which combines convolutional networks with regression frameworks to enhance material property prediction. Prior studies have shown that CNNs, when integrated with ensemble methods or processing metadata, significantly improve generalization and interpretability. For example, Zhang et al. [51] demonstrated that CNNs fused with physical descriptors could accurately predict strength degradation in composite systems. Similarly, Zhao et al. [52] employed CNN hybrids for polymer electrolyte analysis, showcasing superior performance over traditional pipelines. Inspired by these works, our model treats CNN-extracted image features as the primary predictors and can be extended to hybrid configurations in future studies.

4.8. Generalization and Data Augmentation. Considering the relatively small size of the SEM image dataset, we applied several data augmentation techniques—including random rotations, horizontal/vertical flips, brightness and contrast perturbations, and random cropping—to reduce overfitting and enhance model robustness. An ablation study revealed that these transformations had mixed results: swelling prediction marginally improved (MSE reduced from 2.59×10^{-4} to 2.55×10^{-4}), while other properties experienced slight increases in error, indicating that excessive augmentation may introduce noise in limited datasets. Further exploration of synthetic data generation or domain adaptation could help overcome these limitations.

4.9. Summary of Predictive Results. Figure 14 visualizes the performance of the CNN model across material properties. The lowest MSE was achieved for swelling, reflecting strong alignment between predicted and actual weight values. Hardness and tensile strength yielded moderate error, while resistivity remained the most challenging to predict. The results

Table 4: Model performance comparison (MSE).

Material property	CNN MSE	Linear regression MSE	SVR MSE
Tensile strength	7.571e + 01	1.223e + 02	8.892e + 01
Hardness	4.450e + 00	6.130e + 00	5.770e + 00
Resistivity	1.225e + 15	2.036e + 15	1.743e + 15
Swelling	2.200e− 04	3.150e− 04	2.950e− 04

demonstrate that deep convolutional models can effectively learn microstructural cues from image data and support targeted enhancement strategies—such as architectural redesign and preprocessing refinement—for improving predictive outcomes.

We developed a CNN model to predict four material properties—tensile strength, resistivity, weight, and hardness—from grayscale images of materials subjected to varying levels of pressure. A hyperparameter tuning approach was utilized to improve the model's performance, with key parameters such as the number of convolutional layers, the number of filters in each layer, and the learning rate of the optimizer being optimized. The results for each property, evaluated using the MSE metric, are discussed in detail below.

Table 3 summarizes the performance of the CNN model in predicting the material properties under hydrogen exposure. For tensile strength, the model achieved a MSE of 75.71, indicating moderate effectiveness with room for improvement. This error is within an acceptable range, given that the tensile strength values in the dataset range from approximately 59.94–75.97, suggesting the model's predictions are reasonable but could benefit from further refinement. Resistivity prediction yielded an extremely high MSE of 1.225×10^{15}, highlighting significant accuracy shortcomings. This suggests potential overfitting or underfitting, likely due to the large numerical range of resistivity values, and warrants further investigation into preprocessing techniques to improve model performance. In contrast, the model performed exceptionally well in predicting weight, with an MSE of 2.20×10^{-4}. This extremely low error indicates that the model can predict material weight from images with high accuracy. The close alignment between predicted and actual values reflects the model's effectiveness, particularly given the relatively small range of weight values in the dataset (approximately 1.087–1.144). For hardness, the model produced an MSE of 4.45, indicating a moderate level of predictive accuracy. Given that the hardness values range from 74.6 to 78.2, the error is proportionally lower than for tensile strength, indicating reasonable performance. Although the error is not as low as in weight prediction, this outcome is acceptable for an initial model and could be improved with further tuning and additional data.

Figure 14 presents the MSE values for four material properties predicted by the CNN: tensile strength, resistivity, weight, and hardness. The CNN model demonstrated strong predictive capability for weight with a low MSE, indicating consistent data. Hardness showed moderate predictive accuracy with an MSE of 4.45, suggesting room for improvement. Tensile Strength had a higher MSE of 75.71, indicating the need for refinement in predictions. Conversely, resistivity faced

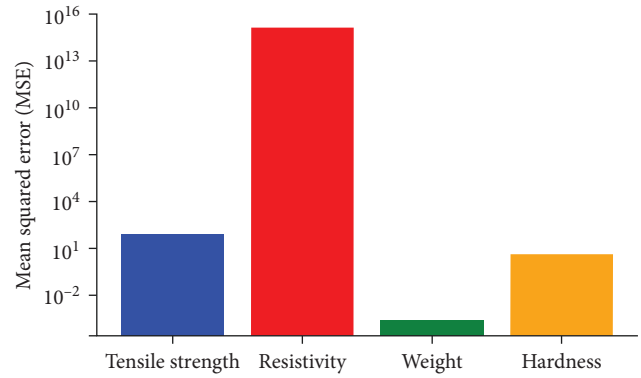

Figure 14: Comparison of MSE for material property predictions using CNN model.

significant challenges, evidenced by an extreme MSE, highlighting the necessity for better preprocessing or feature engineering. Overall, the results underscore the varying effectiveness of the model and the need for targeted strategies to enhance resistivity predictions, while maintaining strength in weight forecasting.

4.10. Hyperparameter Tuning and Model Optimization. The effective optimization of key model hyperparameters, including the number of convolutional layers (ranging from 2 to 4), the number of filters in each layer (32 to 128), and the learning rate of the Adam optimizer (between 0.0001 and 0.01). This approach facilitated a systematic exploration of various hyperparameter combinations, ultimately identifying the model configuration that minimized validation Mean Absolute Error (MAE). The final model was trained for 10 epochs on the training dataset and evaluated on the test set. The model performed well in predicting weight and moderately well in predicting tensile strength and hardness; the prediction of resistivity remains problematic.

5. Discussion

Hydrogen's potential as a clean energy carrier has led to significant advancements in storage and transportation technologies. However, the performance of sealing materials under hydrogen exposure remains a critical challenge due to hydrogen's small molecular size, high diffusivity, and reactivity. These factors can cause material degradation, compromise sealing integrity, and pose safety risks in hydrogen systems. This study focuses on NBR, a widely used sealing material, and investigates its mechanical and morphological behavior under medium-pressure hydrogen exposure through experimental characterization and predictive modeling. The findings contribute to

understanding the factors influencing sealing performance and provide insights into material selection and design for hydrogen energy applications.

Tensile strength, a key mechanical property, reflects a material's ability to resist breaking under tension. This mechanical property is critical for polymers used in sealing applications because it indicates their ability to withstand mechanical stress without failure. Polymers with high tensile strength, such as thermoplastic polyurethanes (TPUs) and thermoplastic vulcanizates (TPVs), exhibit robust molecular structures with strong intermolecular forces and well-entangled molecular chains, which enhance their durability and mechanical performance under stress. The chemical structure of polymers plays a significant role in determining their tensile strength and sealing efficiency. Cross-linked polymers, where polymer chains are interconnected through covalent bonds, display superior tensile strength and sealing resistance due to reduced chain mobility and enhanced structural integrity. For instance, vulcanized rubbers and cross-linked polyethylenes are notable for their high tensile strength and exceptional sealing capabilities. Additionally, the incorporation of fillers like carbon black or silica further strengthens the polymer matrix by enhancing tensile strength, abrasion resistance, and sealing efficiency. Cross-link density is a critical parameter in evaluating a polymer's mechanical performance and sealing capability. A higher cross-link density reduces the permeability of the polymer matrix, thereby improving its ability to withstand high-pressure environments without compromising sealing integrity. This relationship is well captured by models such as the Flory–Rehner equation, which correlates crosslink density with material properties like tensile strength and swelling resistance. In hydrogen applications, where pressure-induced permeation is a significant concern, polymers with high crosslink density are particularly effective in mitigating degradation and maintaining long-term performance. When subjected to pressure, seals need to deform to create a tight seal without rupturing. Polymers with high tensile strength can endure these stresses, providing reliable and durable seals. The mechanical durability of elastomers, evaluated in terms of their tension and compression set (CS) behaviors, shows that materials like TPV maintain their sealing properties better than others, like EPDM, under high-temperature aging conditions.

In the energy industry, sealing materials must meet specific tensile strength requirements to ensure reliability and safety. Generally, a minimum tensile strength of at least 10 MPa is required for sealing applications. However, for high-performance applications, such as those in the hydrogen energy sector, tensile strengths of 20–30 MPa or higher are often necessary. These higher tensile strengths ensure that the seals can withstand extreme pressures, temperatures, and chemical exposures typical in such demanding environments. The predictive model developed in this study can be instrumental for the sealing industry, especially in the hydrogen energy sector. By accurately predicting the tensile strength of polymers based on numerical and image data, the model allows for the assessment of a polymer's suitability for sealing applications without extensive physical testing. This capability is crucial for developing seals that can withstand the unique challenges of hydrogen storage and transportation, including high pressures and low temperatures. The model can expedite the material selection process, reduce costs associated with empirical testing, and enhance the reliability of seals used in hydrogen applications. By ensuring that only polymers with adequate tensile strength are selected, the model helps in designing seals that are both safe and efficient, contributing to the broader adoption of hydrogen as a clean energy source [53, 54]. By leveraging this model, the sealing industry can enhance the development of high-performance seals, ensuring the safe and efficient use of hydrogen as a sustainable energy source.

The findings of this study have several direct applications in hydrogen infrastructure, especially in the design, selection, and maintenance of sealing systems used in hydrogen storage, refueling, and transportation. The observed degradation in tensile strength, hardness, and increased resistivity and swelling under hydrogen pressure exposure demonstrates that conventional NBR formulations may face performance limitations when used in medium- to high-pressure environments (3000–5000 psi). This information is particularly relevant for O-ring and gasket manufacturers, as these components must maintain integrity in hydrogen compressors, pipeline flanges, and refueling couplings. The swelling behavior and microcrack propagation revealed through SEM imaging underscore the importance of pressure-specific material qualification standards, especially as hydrogen embrittlement and leakage can lead to hazardous outcomes in high-risk environments [12, 14]. Furthermore, the predictive models developed, including the CNN-based image-to-property framework, can serve as early diagnostic tools for identifying degraded seals before catastrophic failure. By integrating these models into inspection workflows, maintenance teams in hydrogen refueling stations or electrolyzer facilities can potentially reduce downtime, improve safety, and extend component life. This approach aligns with the ongoing industry efforts to quantify hydrogen compatibility and build robust seal performance databases [24, 25]. This work contributes to standardizing polymer selection for hydrogen systems, informs design engineers on pressure-sensitive performance limits, and provides a path forward for data-driven predictive maintenance strategies in the clean energy sector.

6. Conclusion

This study provides valuable insights into the behavior of NBR seals under medium-pressure hydrogen environments, highlighting the critical challenges associated with material degradation. The experimental analysis revealed notable reductions in tensile strength and hardness, increased resistivity, and swelling due to hydrogen-induced deterioration, accompanied by the development of surface roughening and microcracks. These structural and mechanical changes underscore the vulnerability of NBR in hydrogen applications, emphasizing the importance of enhancing material design for improved sealing performance. The integration of a hybrid machine learning model in this research marks a significant step forward in predicting material performance. By combining numerical features and SEM-based image data, the model achieved high

predictive accuracy for key mechanical properties, enabling efficient evaluation of sealing materials without extensive physical testing. This approach offers a powerful tool for accelerating material development and optimizing seal design to meet the rigorous demands of hydrogen systems.

The findings of this study have meaningful implications for the future of hydrogen infrastructure. They provide a foundation for developing advanced sealing materials capable of maintaining their integrity under high-pressure hydrogen conditions. By improving our understanding of hydrogen-material interactions and leveraging predictive tools, this research contributes to safer and more reliable hydrogen storage and transportation systems. Further studies exploring other material formulations, higher operating pressures, and long-term aging effects will be instrumental in advancing the hydrogen energy sector, supporting its role as a cornerstone of sustainable energy solutions.

Data Availability Statement

The data that supports the findings of this study are available upon request by the corresponding author.

Conflicts of Interest

The authors declare no conflicts of interest.

Funding

Financial support was provided by the University of Oklahoma Libraries' Open Access Fund.

References

[1] S. G. Nnabuife, E. Oko, B. Kuang, et al., "The Prospects of Hydrogen in Achieving Net Zero Emissions by 2050: A Critical Review," *Sustainable Chemistry for Climate Action* 2 (2023): 100024.

[2] A. Pareek, R. Dom, J. Gupta, J. Chandran, V. Adepu, and P. H. Borse, "Insights Into Renewable Hydrogen Energy: Recent Advances and Prospects," *Materials Science for Energy Technologies* 3 (2020): 319–327.

[3] B. Sun, H. Zhao, X. Dong, et al., "Current Challenges in the Utilization of Hydrogen Energy-A Focused Review on the Issue of Hydrogen-Induced Damage and Embrittlement," *Advances in Applied Energy* 14 (2024): 100168.

[4] M. T. Ahad, M. M. H. Bhuiyan, A. N. Sakib, A. Becerril Corral, and Z. Siddique, "An Overview of Challenges for the Future of Hydrogen," *Materials* 16, no. 20 (2023): 6680.

[5] S. Bosu and N. Rajamohan, "Recent Advancements in Hydrogen Storage - Comparative Review on Methods, Operating Conditions and Challenges," *International Journal of Hydrogen Energy* 52 (2024): 352–370.

[6] M. M. H. Bhuiyan and Z. Siddique, "Hydrogen as an Alternative Fuel: A Comprehensive Review of Challenges and Opportunities in Production, Storage, and Transportation," *International Journal of Hydrogen Energy* 102 (2025): 1026–1044.

[7] A. N. Sakib, F. Mehjabin, J. B. Schmidt, M. Haque, K. Saha, and M. M. H. Bhuiyan, "Harnessing Hydrogen: A Comprehensive Literature Review on Strategic Launching Initiatives in the Global Energy Market," *International Journal of Energy Research* 2024, no. 1 (2024): 3265065.

[8] U. S. Meda, N. Bhat, A. Pandey, K. N. Subramanya, and M. A. Lourdu Antony Raj, "Challenges Associated With Hydrogen Storage Systems Due to the Hydrogen Embrittlement of High Strength Steels," *International Journal of Hydrogen Energy* 48, no. 47 (2023): 17894–17913.

[9] C. Zhou, H. Zhou, and L. Zhang, "The Impact of Impurity Gases on the Hydrogen Embrittlement Behavior of Pipeline Steel in High-Pressure H2 Environments," *Materials* 17, no. 9 (2024): 2157.

[10] H. Barthélémy, "Effects of Pressure and Purity on the Hydrogen Embrittlement of Steels," *International Journal of Hydrogen Energy* 36, no. 3 (2011): 2750–2758.

[11] S. S. Kulkarni, K. S. Choi, W. Kuang, et al., "Damage Evolution in Polymer Due to Exposure to High-Pressure Hydrogen Gas," *International Journal of Hydrogen Energy* 46, no. 36 (2021): 19001–19022.

[12] C. Zhou, Y. Huang, Y. Zheng, and Z. Hua, "Hydrogen Permeation Behavior of Rubber Sealing Materials for Hydrogen Infrastructure: Recent Advances and Perspectives," *International Journal of Hydrogen Energy* 59, no. 2024 (2024): 742–754.

[13] H. Ono, H. Fujiwara, and S. Nishimura, "Penetrated Hydrogen Content and Volume Inflation in Unfilled NBR Exposed to High-Pressure Hydrogen–What Are the Characteristics of Unfilled-NBR Dominating Them?" *International Journal of Hydrogen Energy* 43, no. 39 (2018): 18392–18402.

[14] M. Calabrese, M. Portarapillo, A. Di Nardo, et al., "Hydrogen Safety Challenges: A Comprehensive Review on Production, Storage, Transport, Utilization, and CFD-Based Consequence and Risk Assessment," *Energies* 17, no. 6 (2024): 1350.

[15] M. M. H. Bhuiyan, A. N. Sakib, A. B. Corral, and Z. Siddique, "Investigating the Influence of Operating Variables on Sealing Performance of a V-Ring Seal Stack in the Oil and Gas Industry for Enhanced Environmental and Operational Performance," *SSRN Electronic Journal* 131 (2023): 108346.

[16] N. Menon, A. Kruizenga, K. J. Alvine, C. S. Marchi, A. Nissen, and K. Brooks, "Behaviour of Polymers in High Pressure Environments as Applicable to the Hydrogen Infrastructure," in *Sandia National Lab (SNL-CA)*, (Livermore, CA(United States), https://www.osti.gov/servlets/purl/1404764, 2016).

[17] C. Zhou, J. Zheng, C. Gu, Y. Zhao, and P. Liu, "Sealing Performance Analysis of Rubber O-Ring in High-Pressure Gaseous Hydrogen Based on Finite Element Method," *International Journal of Hydrogen Energy* 42, no. 16 (2017): 11996–12004.

[18] L. Kumar and A. K. Sleiti, "A Comprehensive Review of Hydrogen Safety Through a Metadata Analysis Framework," *Renewable and Sustainable Energy Reviews* 214 (2025): 115509.

[19] H. Li, X. Cao, Y. Liu, et al., "Safety of Hydrogen Storage and Transportation: An Overview on Mechanisms, Techniques, and Challenges," *Energy Reports* 8 (2022): 6258–6269.

[20] R. R. Barth, K. L. Simmons, and C. San Marchi, "Polymers for Hydrogen Infrastructure and Vehicle Fuel Systems: Applications, Properties, and Gap Analysis," in *Sandia National Laboratories (SNL-CA)*, (Livermore, CA, USA, 2013).

[21] X. Zhang, X. Xie, H. Zhao, et al., "Seismic Response Prediction Method of Train-Bridge Coupled System Based on Convolutional Neural Network-Bidirectional Long Short-Term Memory-Attention Modeling," *Advances in Structural Engineering* 28, no. 2 (2025): 341–357.

[22] X. Zhang, X. Xie, S. Tang, et al., "High-Speed Railway Seismic Response Prediction Using CNN-LSTM Hybrid Neural

Network," *Journal of Civil Structural Health Monitoring* 14, no. 5 (2024): 1125–1139.
[23] J. G. Speight, "Monomers, Polymers, and Plastics," in *Speight, Handbook of Industrial Hydrocarbon Processes*, Second Edition ed., ed. G. James, (Gulf Professional Publishing, 9780128099230, 2020): 597–649.
[24] K. L. Simmons, W. Kuang, S. D. Burton, et al., "H-Mat Hydrogen Compatibility of Polymers and Elastomers," *International Journal of Hydrogen Energy* 46, no. 23 (2021): 12300–12310.
[25] Y. Zheng, Y. Tan, C. Zhou, et al., "A Review on Effect of Hydrogen on Rubber Seals Used in the High-Pressure Hydrogen Infrastructure," *International Journal of Hydrogen Energy* 45, no. 43 (2020): 23721–23738.
[26] A. A. Abdelsalam, S. Araby, S. H. El-Sabbagh, A. Abdelmoneim, and M. A. Hassan, "Effect of Carbon Black Loading on Mechanical and Rheological Properties of Natural Rubber/Styrene-Butadiene Rubber/Nitrile Butadiene Rubber Blends," *Journal of Thermoplastic Composite Materials* 34, no. 4 (2021): 490–507.
[27] M. H. Al-maamori, A. A.-A. Al-Zubaidi, and A. A. Subeh, "Effect of Carbon Black on Mechanical and Physical Properties o fAcrylonitrile Butadiene Rubber (NBR) Composite," *Academic Research International* 6, no. 2 (2015).
[28] W. Balasooriya, C. Clute, B. Schrittesser, and G. Pinter, "A Review on Applicability, Limitations, and Improvements of Polymeric Materials in High-Pressure Hydrogen Gas Atmospheres," *Polymer Reviews* 62, no. 1 (2022): 175–209.
[29] A. N. Sakib, *Enhancing Hydrogen Energy Storage and Transportation Systems: Predictive Modeling of Sealing Materials Through Ex-Situ Experimental Analysis*, (https://www.proquest.com/openview/072613b0a80ae956191161efeb9a4a23/1?pq-origsite=gscholar&cbl=18750&diss=y, University of Oklahoma – Graduate College ProQuest Dissertations & Theses, 2024).
[30] G. Sachs, "Carbonomics: The Rise of Clean Hydrogen," (2020).
[31] Y. Liu, W. Guo, X. Zhu, and S. Yu, "Effect of Hydrothermal Aging on the Tribological Performance of Nitrile Butadiene Rubber Seals," *Polymers* 13, no. 4 (2021): 658.
[32] American Society for Testing and Materials, *Standard Test Method for Tensile Properties of Plastics* (PA: ASTM International, West Conshohocken, 2014, https://www.astm.org/d0638-14.html.
[33] M. F. Abdelkarim, L. S. Nasrat, S. M. Elkhodary, A. M. Soliman, and A. M. Hassan, "Volume Resistivity and Mechanical Behavior of Epoxy Nanocomposite Materials," *Polymers* 13, no. 4 (2021): 658.
[34] A. Al-Awadhi, M. Taha, and Z. Saleem, "Volume Resistivity of Viton Polymer Under Thermal Aging," *Polymers* 13, no. 4 (2021), https://www.mdpi.com/2073-4360/13/4/658: 658.
[35] H. Reingruber, A. Zankel, C. Mayrhofer, and P. Poelt, "A New in Situ Method for the Characterization of Membranes in a Wet State in the Environmental Scanning Electron Microscope," *Journal of Membrane Science* 399-400 (2012): 86–94.
[36] S. A. Khan, S. B. Khan, and A. M. Asiri, "Scanning Electron Microscopy: Principle and Applications in Nanomaterials Characterization," *Journal of Materials Science: Materials in Electronics* 27 (2016): 5294–5302.
[37] S. F. Grebennikov, A. N. Aitova, and E. S. Abramova, "Thermodynamics of Swelling in Glassy Amorphous/Crystalline Polymers in Water Vapor," *Fibre Chemistry* 50, no. 3 (2018): 179–187.
[38] A. Sienkiewicz, P. Krasucka, B. Charmas, W. Stefaniak, and J. Goworek, "Swelling Effects in Cross-Linked Polymers by Thermogravimetry," *Journal of Thermal Analysis and Calorimetry* 130, no. 1 (2017): 85–93.
[39] J. P. E. Grolier and S. A. E. Boyer, "Gas–Polymer Interactions: Key Thermodynamic Data and Thermophysical Properties," in *Polymer Thermodynamics. Advances in Polymer Science*, ed. B. Wolf and S. Enders, 238, (Springer, Berlin, Heidelberg, 2010).
[40] S. K. Jeon, J. K. Jung, N. K. Chung, U. B. Baek, and S. H. Nahm, "Investigation of Physical and Mechanical Characteristics of Rubber Materials Exposed to High-Pressure Hydrogen," *Polymers* 14, no. 11 (2022): 2233.
[41] S. Y. Lee, S. B. Eom, J. S. Won, J. W. Bae, S. H. Park, and S. G. Lee, "Evaluation of Aging Behavior of Nitrile Butadiene Rubbers Via Oxygen-Consumption Experiments," *Fibers and Polymers* 22, no. 3 (2021): 639–646.
[42] S. P. Ammineni, D. Lingaraju, and C. Nagaraju, "The Effects of Physical Aging on the Quasi-Static and Dynamic Viscoelastic Properties of Nitrile Butadiene Rubber," *Mechanics of Time-Dependent Materials* 27, no. 3 (2023): 765–789.
[43] H. Fujiwara, "Analysis of Acrylonitrile Butadiene Rubber (NBR) Expanded With Penetrated Hydrogen Due to High-pressure Hydrogen Exposure," *Nippon Gomu Kyokaishi* 89, no. 10 (2016): 295–301.
[44] G. Theiler, N. C. Murillo, and A. Hausberger, "Effect of Hydrogen Pressure on the Fretting Behavior of Rubber Materials," *Lubricants* 12, no. 7 (2024): 233.
[45] J. Sterr, B. S. Fleckenstein, and H.-C. Langowski, "The Theory of Decompression Failure in Polymers During the High-Pressure Processing of Food," *Food Engineering Reviews* 10, no. 1 (2018): 14–33.
[46] B. Flaconneche, J. Martin, and M. H. Klopffer, "Permeability, Diffusion and Solubility of Gases in Polyethylene, Polyamide 11 and Poly (Vinylidene Fluoride)," *Oil & Gas Science and Technology* 56, no. 3 (2001): 261–278.
[47] T. Michler, K. Wackermann, and F. Schweizer, "Review and Assessment of the Effect of Hydrogen Gas Pressure on the Embrittlement of Steels in Gaseous Hydrogen Environment," *Metals* 11, no. 4 (2021): 637.
[48] J. K. Jung, I. G. Kim, and K. T. Kim, "Evaluation of Hydrogen Permeation Characteristics in Rubbery Polymers," *Current Applied Physics* 21 (2021): 43–49.
[49] H2Tools Technical Reference for Hydrogen Compatibility of Polymers, https://h2tools.org/sites/default/files/8100TechRef_polymers.pdf.
[50] UNT Digital Library, "Hydrogen Absorption in Polymers: Permeability, Solubility, and Interaction With Elastomers," "U.S. Department of Energy," 2010, https://digital.library.unt.edu/ark:/67531/metadc902701/m2/1/high_res_d/927901.pdf.
[51] H. Zhang, H. Yin, X. Lei, et al., "An Improved CNN-Based Algorithm for Quantitative Prediction of Impact Damage Depth in Civil Aircraft Composites via Multi-Domain Terahertz Spectroscopy," *Electronics* 14, no. 12 (2025): 2412.
[52] Z. Zhao, L. Liu, and W. Zhang, "CNN Hybrid Models for Polymer Electrolyte Analysis," 2024, https://arxiv.org/abs/2409.02952.
[53] J. Kim, S. Lee, J. Park, S. Choi, and S. Hwang, "Mechanical Aging Test and Sealing Performance of Thermoplastic Vulcanizate as Sealing Gasket in Automotive Fuel Cell Applications," *Polymers* 13, no. 11 (2021): 1785.
[54] Huntsman Guide to Thermoplastic Polyurethanes (TPUs), Available at: [Huntsman Guide] https://huntsmanpimcore.equisolvedev.com/Documents/PU_Elastomers_Guide_to_TPU.pdf.